Circuits Syst Signal Process (2011) 30: 55–71
DOI 10.1007/s00034-010-9207-3

A New Method for the Estimation of Mass Functions in the Dempster–Shafer's Evidence Theory: Application to Colour Image Segmentation

Salim Ben Chaabane · Mounir Sayadi · Farhat Fnaiech · Eric Brassart · Franck Betin

Received: 19 December 2008 / Revised: 26 February 2010 / Published online: 17 September 2010

Abstract In this paper, the problem of colour image segmentation is addressed using the Dempster–Shafer (DS) theory. Examples are provided showing that this theory is able to take into account a large variety of special situations that occur and which are not well solved using classical approaches. Modelling both uncertainty and imprecision, and computing the conflict between images and introducing a priori information are the main features of this theory. Consequently, the performance of such a segmentation scheme is largely conditioned by the appropriate estimation of mass functions in the DS evidence theory. In this paper, a new method of automatically determining the mass function for colour-image segmentation problems is presented. The mass function of each pixel is determined by applying possibilistic c-means (PCM) clustering to the grey levels of the three primitive colours. A reliability criterion, associ-

S. Ben Chaabane (✉) · M. Sayadi · F. Fnaiech
SICISI Unit, ESSTT, University of Tunis, 5 Av. Taha Hussein, 1008 Tunis, Tunisia
e-mail: ben_chaabane_salim@yahoo.fr

M. Sayadi
e-mail: mounirsayadi@yahoo.fr

F. Fnaiech
e-mail: fnaiech@ieee.org

M. Sayadi · F. Fnaiech · E. Brassart · F. Betin
Laboratory for Innovation Technologies (LTI-UPRES EA3899), Electrical Power Engineering Group (EESA), University of Picardie Jules Verne, 7, rue du Moulin Neuf, 80000 Amiens, France

E. Brassart
e-mail: eric.brassart@u-picardie.fr

F. Betin
e-mail: franck.betin@u-picardie.fr

F. Fnaiech
ETS, Dept. Elec. Eng, Univ. Quebec at Montréal, 1100 Rue Notre Dame ouest, Montreal, H3C1K3 Quebec, Canada

ated with each pixel and the mass functions of its neighbouring pixels, is used into a fuzzy based reasoning system in order to decide on the appropriate segmentation. Experimental segmentation results on medical and textured colour images highlight the effectiveness of the proposed method.

Keywords Dempster–Shafer's evidence theory · Data fusion · Conflict · Fuzzy clustering · Possibilistic approaches

1 Introduction

Data fusion techniques [3], based on exploiting redundant and complementary information from different sources is an appealing approach for colour image segmentation [10, 11, 23, 26]. Many approaches or mathematical formalisms have been proposed for data fusion: probability [27], fuzzy logic [2, 20, 24], possibilities [13], evidence theory [14, 28], etc.

Moreover, the Dempster–Shafer evidence theory aims to represent and handle uncertain information. An important property of this theory is its ability to merge different data sources in order to increase the information quality. The application areas of the DS theory are various [15, 20], but in the use of this theory for image segmentation, the determination of the mass functions is a hard task. Many authors have addressed this problem using different approaches [25, 29, 31, 32]. In particular, the relationship between the fuzzy sets and the DS evidence theory is investigated in [4, 30]. In terms of using the evidence theory for image segmentation application, due to the deficiency of specificity and the fuzziness of the mass function estimation in the evidence theory, the advantages provided by fuzzy set theory are characterized by various definitions of membership functions.

In this context, Zimmermann and Zysno [31] have provided a model for membership functions based on the "distance" of a point from a prototypical member (MMFD). However, one of the major factors that influences the determination of the membership functions is the "distance measure" chosen for the problem at hand [6, 31]. With the same objective, Vannoorenberghe et al. [29] have shown through empirical studies that a good model of the mass functions is based on the assumption of *Gaussian distributions* (MMFAGD) and histogram thresholding and applied on synthetic and biomedical images that contain only two classes. However, this model-based method requires the knowledge of a priori information not often available at our disposal. Hence, Ben Chaabane et al. [7, 8] proposed a mass functions estimation based on fuzzy homogeneity approach to overcome this limitation. This method may be seen to be a straightforward complement to that in the paper proposed by Vannoorenberghe et al. [29].

Recently, fuzzy clustering methods have shown good ability to generate the membership update equations for an iterative algorithm. Most analytic fuzzy approaches are derived from Bezdek's Fuzzy C-Means (FCM) algorithm applied to the grey levels to automatically determine the membership degree of each pixel. The idea is to assign, at each image pixel level, a mass function that corresponds to a membership function in fuzzy logic [9, 32]. The degrees of membership of the various pixels are

determined by applying fuzzy c-means (FCM) clustering to the grey levels of the image.

However, this algorithm has a considerable difficulty in noisy environments, and the memberships resulting from FCM do not always correspond to the intuitive concept of degree of belonging or compatibility. The membership degrees are computed using only the grey levels and do not take into account the spatial information of pixels with respect to one another. Also, the Hard C-Means (HCM) [16] is one of the oldest clustering methods in which HCM memberships are hard (i.e., 1 or 0). This method is used to learn the prototypes of clusters or classes, and the cluster's centres are used as prototypes. In principle, the main differences between the various works in the references cited above are in the method of mass functions estimation, and in the application. At the same time, one should point out the lack of methods for automatically generating the membership functions from the training data; this is a serious problem in many applications.

In this paper, we investigate as to how the user can choose a suitable method for determining the mass function in the Dempster–Shafer evidence theory. We reformulate the fuzzy clustering problem so that the clustering method can be used to generate memberships with typical interpretation. Hence, this work may be seen as a straightforward complement to the one proposed by Zhu et al. [32]. In their paper, the authors suggested that the user has to search for a suitable method for automatically determining the mass function. Hence, this paper is devoted to this task, applied to colour image segmentation, where we aim at providing help to the doctor for the follow-up of the diseases of the breast cancer. The objective is to rebuild each cell from a series of three component images (R, G and B). From an initial segmentation obtained by using the PCM algorithm, one seeks a segmentation which represents as well as possible the cells, in order to give to the doctors a schema of the points really forming part of the cells, as also the number of the cells. The idea is based on the Possibilistic C-Means (PCM) algorithm. The determination of the mass function does not only take into account the advantage of the fuzzy framework, but also considers the spatial relation of the membership degrees among neighbouring pixels to explore the image features. Once the mass functions are determined for each primitive colour to be fused, the DS combination rule and decision are applied to obtain the final segmentation.

Section 2 introduces a method for the estimation of the mass functions in the Dempster–Shafer evidence theory, as applied to colour image segmentation. Experimental results are discussed in Sect. 3, and conclusion is given in Sect. 4.

2 Mass Functions Determination Using PCM

The original FCM formulation minimizes the objective function given by [5]:

$$J_{\mathrm{FCM}} = J_m(u, v) = \sum_{i=1}^{c} \sum_{k=1}^{n} u_{ik}^m d_{ik}^2 \tag{1}$$

subject to $\sum_{i=1}^{c} u_{ik} = 1$ for all k.

In (1), d_{ik}^2 is the distance of the feature point x_k to the centres of the classes v_i of an $(M \times N)$ image, $n = M \times N$ is the total number of feature vectors, c is the number of classes that are user-dependent and should be known a priori in the PCM algorithm, and $U = [u_{ik}]$ is a $c \times n$ matrix, called the fuzzy c-partition matrix [1, 19, 21, 22], u_{ik} is the membership degree of the feature point x_k in cluster i, and $m \in [1, \infty]$ is a weighting exponent called the fuzzifier.

Simply relaxing the constraint in (1) produces a trivial solution, i.e., the criterion function is minimized by assigning all membership to zero. Clearly, one would like to have a good possibilistic data partition (high membership for the representative points and low membership for the unrepresentative ones). The objective function which satisfies these hypotheses may be formulated as [25]:

$$\begin{aligned} J_{\mathrm{PCM}} &= J_m(u, v) \\ &= \sum_{k=1}^{n}\sum_{i=1}^{c} u_{ik}^m d_{ik}^2 + \sum_{k=1}^{n} \eta_k \sum_{i=1}^{c} (1 - u_{ik})^m \end{aligned} \tag{2}$$

where η_k are suitable positive numbers. The first term requires that the distances from the vectors of the prototypes be as low as possible, whereas the second term forces the u_{ik} to be as large as possible: this avoids the trivial solution.

The necessary conditions on the prototypes are identical to the corresponding conditions in the FCM and its derivatives.

Hence, minimizing J_{PCM} with respect to U is equivalent to minimizing the following objective function (2), with respect to each one of the u_{ik}:

$$J_{\mathrm{PCM}} = u_{ik}^m d_{ik}^2 + \eta_k (1 - u_{ik})^m. \tag{3}$$

Differentiating (3) with respect to u_{ik} and setting it to zero leads to the equation

$$u_{ik} = \frac{1}{1 + (\frac{d_{ik}^2}{\eta_k})^{1/m-1}}. \tag{4}$$

Also, it has to be noted that η_k determines the relative degree to which the second term in the objective function (3) is significant compared to the first term.

If both terms are to be weighted roughly equally, then η_k should depend on d_{ik}^2 with $m = 2$ and

$$\eta_k = \frac{\sum_{k=1}^{n} u_{ik}^m d_{ik}^2}{\sum_{k=1}^{n} u_{ik}^2}. \tag{5}$$

So, we propose a family of possibilistic clustering algorithm of the general form:

The Possibilistic C-Means (PCM) algorithm
Fix the number of clusters c; fix m, $1 < m$;
Set iteration counter $t' = 1$;
Initialize the possibilistic C-partition $U^{(0)}$;
Estimate η_k using (5);
Repeat
Update the prototypes using $U^{(t')}$; as indicated below;
Compute $U^{(t'+1)}$ using (4);
Increment t;
Until $\|U^{(t'-1)} - U^{(t')}\| < \varepsilon$;

where ε is a chosen error. In the present study, the number of clusters is fixed, the value of m is set to 2, and the clustering process is stopped when $\varepsilon \leq 10^{-3}$.

The purpose of segmentation is to partition the image into homogeneous regions. The idea of using the DS evidence theory for image segmentation is to fuse, one by one, the pixels coming from the three images. The PCM is applied to the three primitive colours. Then, the segmented results are combined using the Dempster–Shafer evidence theory to obtain the final segmentation results. In fact, the membership functions generated by PCM clustering do not contain any spatial information, and they are thus sensitive to undesired factors such as noise. To reduce the influence of the undesired factors on the final determination of the mass functions, the spatial neighbourhood is taken into account for the membership functions of each pixel of the images.

However, a final membership degree of each pixel can be regarded as an angle-related function that contains the spatial information among neighbouring pixels. In Fig. 1, eight neighbouring pixels of distance one are angularly related to pixel p_{xy} at the location (x, y) in the window w_{xy}.

Assume that g_{xy} is the intensity of a pixel p_{xy} at the location (x, y) in an $(M \times N)$ image, w_{xy} is a size $(t \times t)$ window centred at pixel (x, y). One could average the resulting membership degrees u_{xy} along the direction θ within the window w_{xy} to

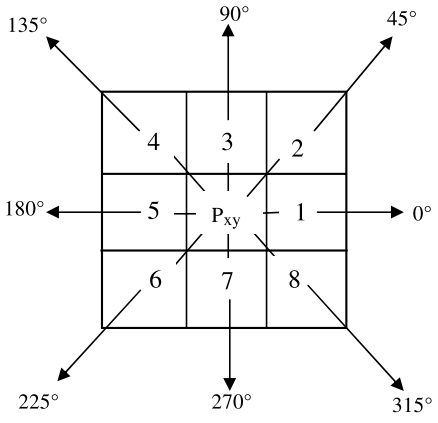

Fig. 1 Spatial relationship between pixel p_{xy} at the location (x, y) and its neighbours in the bloc w_{xy} with different angular θ. Here, the neighbouring distance $d = 1$ and $\theta = \{0°, 45°, 90°, 135°, 180°, 225°, 270°, 315°\}$

obtain a final membership degree $\overline{u}_{xy}$ of each pixel p_{xy}, which will reduce the effect of noise.

The final membership of pixel p_{xy} within the window w_{xy} is computed by

$$\overline{u_{xy}} = \frac{1}{t^2} \sum_{p=x-(t-1)/2}^{x+(t-1)/2} \sum_{q=y-(t-1)/2}^{y+(t-1)/2} u_{pq} \tag{6}$$

where $x \geq 2$, $p \leq M-1$, $y \geq 2$ and $q \leq N-1$.

However, the size of the window has an effect on the computation of the final membership value. The window should be big enough to allow sufficient information provided to the computation of each pixel membership degree. Furthermore, using a larger window in the computation of the membership degree decreases the effect of the noise. Also, a larger window causes a significant processing time. As a trade-off choice, experimentally a (3×3) window is chosen for computing the final membership degree off the final pixel p_{xy}.

However, in the present study, we apply the PCM approach to the three primitive colours (RGB) to represent each grey level g_{xy} by a membership degree $\overline{u_{xy}}$. Then, the segmentation results of the three primitive colours are combined by using the Dempster–Shafer evidence theory [14, 28]. The main advantage of this theory is to affect a degree of confidence, which is called the mass function, to all simple and composed hypotheses (set classes C_i in the present case), and to take into account the lack of information.

Therefore, the clusters generated by the PCM clustering from the frame of discernment Ω composed of i single mutually exclusive subsets H_i is symbolized by

$$\Omega = \{H_1, H_2, \ldots, H_c\} = \{C_i\}; \quad 1 \leq i \leq c. \tag{7}$$

In order to express a degree of confidence for each proposition A of 2^{Ω}, it is possible to associate an elementary mass function $m(A)$ which indicates all confidence that one can have in this proposition. The function m is defined from 2^{Ω} to [0, 1] verifying

$$\begin{cases} m(\phi) = 0, \\ \sum_{A_n \subseteq \Omega} m(A) = 1. \end{cases} \tag{8}$$

If $m(A) > 0$, A is called a focal element.

The main advantage of the DS theory is its robustness of combining information coming from various sources with the DS orthogonal rules [14], given by (10).

Let us assume the presence of Q distinct and independent information sources. Each source is characterized by a mass function defined on the frame of discernment Ω. The Dempster's combination consists in determining the single masse $m(.)$ resulting from the fusion of these Q mass functions $m^Q(.)$ by using the orthogonal rule. Then, the DS combination can be represented for Q information sources by the following orthogonal rule:

$$m(H_i) = m^1(H_i) \oplus m^2(H_i) \oplus \cdots \oplus m^Q(H_i) \tag{9}$$

where $\oplus$ is the sum of DS orthogonal rule.

In the case of two sources S_r and S_s, the DS combination can be represented as

$$\forall H_i \subseteq \Omega, \quad m(H_i) = \frac{1}{K} \sum_{A \cap B = H_i} m^r(A).m^s(B) \tag{10}$$

where K is defined by [14]:

$$K = 1 - \sum_{A \cap B = \phi} m^r(A) m^s(B). \tag{11}$$

Note that this operation is commutative and associative. In (11), the normalization coefficient K evaluates the conflict between the two sources S_r and S_s. The DS theory of evidence is a rich model of uncertainty handling as it allows the expression of partial belief [28].

2.1 Mass Function of Simple Hypotheses

The mass of simple hypotheses H_i is directly obtained from the membership functions $\overline{u_{xy}}$ of the grey level g_{xy} at location (x, y) to cluster i as follows:

$$m_{xy}(H_i) = m_{xy}(C_i) = \overline{u_{xy}}(C_i); \quad 1 \leq i \leq c. \tag{12}$$

2.2 Mass Function of Double Hypotheses

The mass function assigned to double hypotheses depends on the mass functions of each hypothesis. In fact, if there is a high ambiguity in assigning a grey level g_{xy} to cluster C_l or C_m from the same information source, that is $|\overline{u_{xy}}(C_l) - \overline{u_{xy}}(C_m)| < \varepsilon_1$, where ε_1 is a threshold value, then a double hypothesis H_{lm} is formed and its associated mass is computed according to the following formula:

$$\begin{aligned} m_{xy}(H_{lm}) &= m_{xy}(H_l \cup H_m) \\ &= m_{xy}(C_l \cup C_m) \\ &= \hbar\big(\overline{u_{xy}}(C_l), \overline{u_{xy}}(C_m)\big); \quad 1 \leq l, m \leq c \end{aligned} \tag{13}$$

where $\hbar$ denotes a mass function operator, and the value of the threshold ε_1 is chosen following the application in question. In all cases, for the present study, ε_1 is fixed at 0.1.

However, the mass assigned to a double hypothesis depends on the membership degrees of both the simple hypotheses.

It is evident that the more $\overline{u_{xy}}(C_l)$ or $\overline{u_{xy}}(C_m)$ is important, the more the mass to their union is. At the same time, the closer the values of $\overline{u_{xy}}(C_l)$ and $\overline{u_{xy}}(C_m)$ are, the greater is the ambiguity between the two hypotheses forming their union, and consequently, the greater is the mass to assign to the double hypothesis $H_l \cup H_m$.

In the present study, $\hbar$ represents the surface of a triangle presented in Fig. 2. The surface of such a triangle depends on the amplitudes of the membership functions of g_{xy} to the clusters C_l and C_m, and also on the difference between these amplitudes.

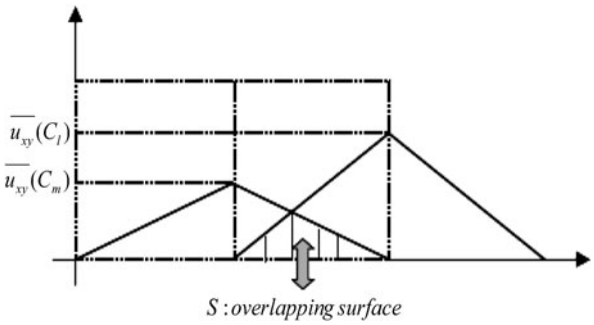

Fig. 2 Construction of triangular membership functions and determination of the overlapped surface

Figure 2 shows how the triangle is constructed and how the mass of double hypothesis $H_l \cup H_m$ is derived from the surface of the triangle. The vertical axis in Fig. 2 represents the membership degrees. The unit of the horizontal has no effect on the mass computation. The heights of the triangles are equal to $\overline{u_{xy}}(C_l)$ and $\overline{u_{xy}}(C_m)$, respectively. The overlapping surface, as represented by the shaded region S in Fig. 2 of the two triangles, represents the membership of a grey level to the composite hypothesis $H_l \cup H_m$ in the new reference system. Therefore, the mass value attributed to the double hypothesis $H_l \cup H_m$(or $C_l \cup C_m$) can be directly computed from the surface S.

From the membership function plots of H_l and H_m(Fig. 2), it can be seen that the highest ambiguity between the hypotheses C_l and C_m is obtained when $\overline{u_{xy}}(C_l) = \overline{u_{xy}}(C_m) = 0.5$. Therefore, we conclude that the maximum of the overlapped surface S corresponds to the highest ambiguity case, and $\overline{u_{xy}}(C_l) = 1$, $\overline{u_{xy}}(C_m) = 0$ correspond to the case of no ambiguity between the two classes.

From the membership functions of hypotheses H_l and H_m, the mass value assigned to the composite hypothesis $H_l \cup H_m$ is then given by

$$\begin{aligned} m_{xy}(H_l \cup H_m) &= m_{xy}(C_l \cup C_m) \\ &= \hbar\big(\overline{u_{xy}}(C_l), \overline{u_{xy}}(C_m)\big) \\ &= \frac{S(\overline{u_{xy}}(C_l)).S(\overline{u_{xy}}(C_m))}{4.S_{\max}}. \end{aligned} \tag{14}$$

From (14), we see that the choice of the geometric shape of the surface has no effect on the final results. The only important values are $\overline{u_{xy}}(C_l)$ and $\overline{u_{xy}}(C_m)$. Thus, the distance between the vertices of the two triangles can be set to 1 for simplification.

Once the mass functions of the three primitive colours (three information sources) are estimated, their combination is performed using the orthogonal sum of the Dempster–Shafer evidence theory that can be represented as follows:

$$m_{xy}(H_i) = m^1_{xy}(H_i) \oplus m^2_{xy}(H_i) \oplus m^3_{xy}(H_i). \tag{15}$$

The decisional procedure for the classification purpose consists of choosing one of the maximum plausibility, the maximum belief, etc., as the most likely hypothesis H_i. The decision-making is carried out on simple hypotheses that represent the classes in the images. If we accept the composite hypotheses as the final results in the

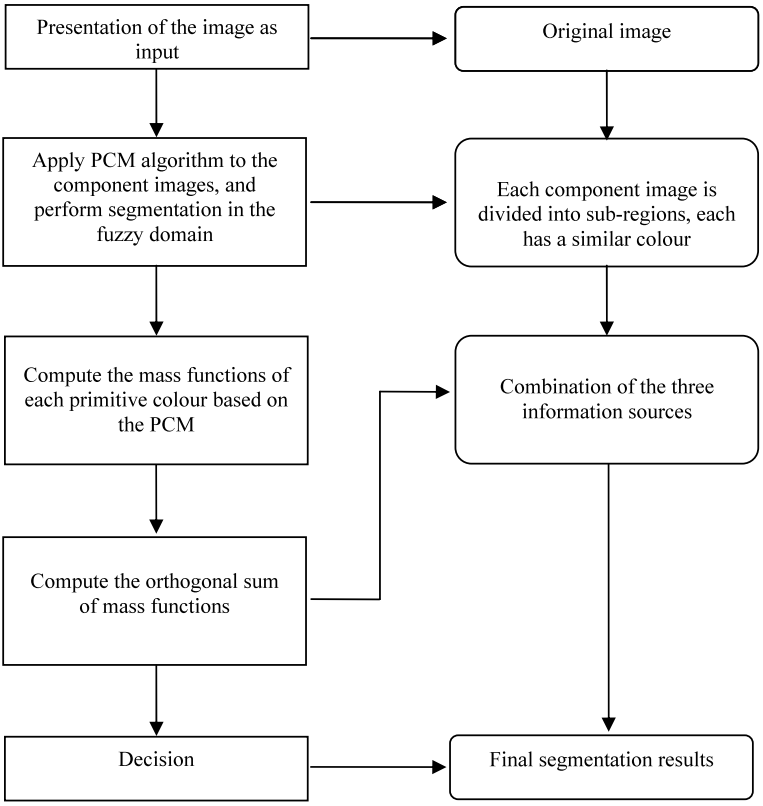

Fig. 3 Flow chart of the proposed method

decisional procedure, the segmentation results obtained would be more reliable but with a decreased precision. The proposed method can be described by the flow chart given in Fig. 3.

3 Experimental Results

In order to illustrate the methods presented in the previous section, a large variety of medical and synthetic colour images (Fig. 4) are employed in our experiments. Some experimental results are shown in Figs. 5–7. The images originally are stored in RGB format. Each of the primitive colours (red, green and blue) is represented by 8 bits and has an intensity range from 0 to 255.

We first present the segmentation results in the RGB colour space by applying the PCM algorithm to the red, green and blue colour features, respectively. In this case, a region is recognized in red component but is not identified by green and blue components. This shows that the RGB space has a strong correlation of its three components, and hence, the use of a single information source leads to bad results.

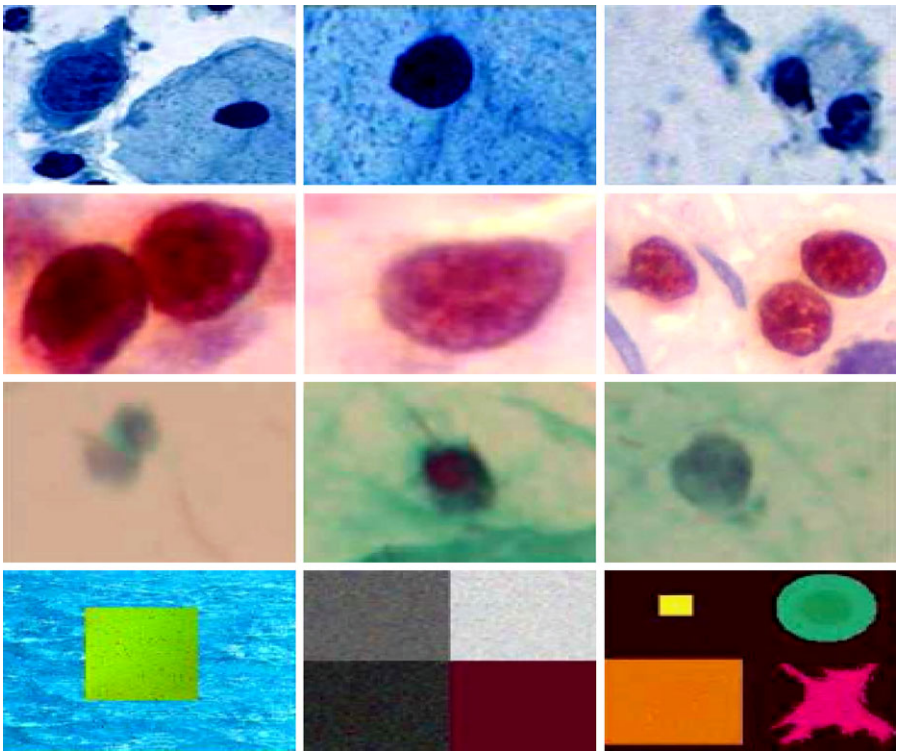

Fig. 4 Data set used in the experiment. Twelve images were selected for a comparison study. The patterns are numbered from 1 to 12, starting at the upper left-hand corner

The experimentation is carried out on medical images of cancer disease type in Fig. 5(a) and these images are used as original images. The results are shown in Figs. 5(b), (c), and (d).

The problem of incorrect segmentation can also be observed in Fig. 5. Indeed, in Fig. 5(b), the resulting image presents six cells, and in Figs. 5(c) and (d) the resulting images present, respectively, only three and five cells.

Comparing the results, we can find that the cells are much better segmented in (b) than those in (c) and (d). Also, the first resulting image contains some holes in one of the cells, which do not exist in another resulting image. This demonstrates the necessity of the fusion process.

For purpose of comparison, we apply the proposed approach and some classical and automatic approaches to the same-colour image segmentation. The latter methods include those of Zimmermann and Zysno [31], Ben Chaabane et al. [6], Vannoorenberghe et al. [29], Zhu et al. [32] and Duda and Hart [16]. The segmentation results are shown in Figs. 6 and 7.

Figure 6 shows a comparison of the results between the traditional methods MMFD [31], MMFADG [29], and the proposed method. The segmentation results are obtained using the MMFD, the MMFAGD and PCM clustering algorithms for the determination of the mass functions in the DS theory. They correspond, respec-

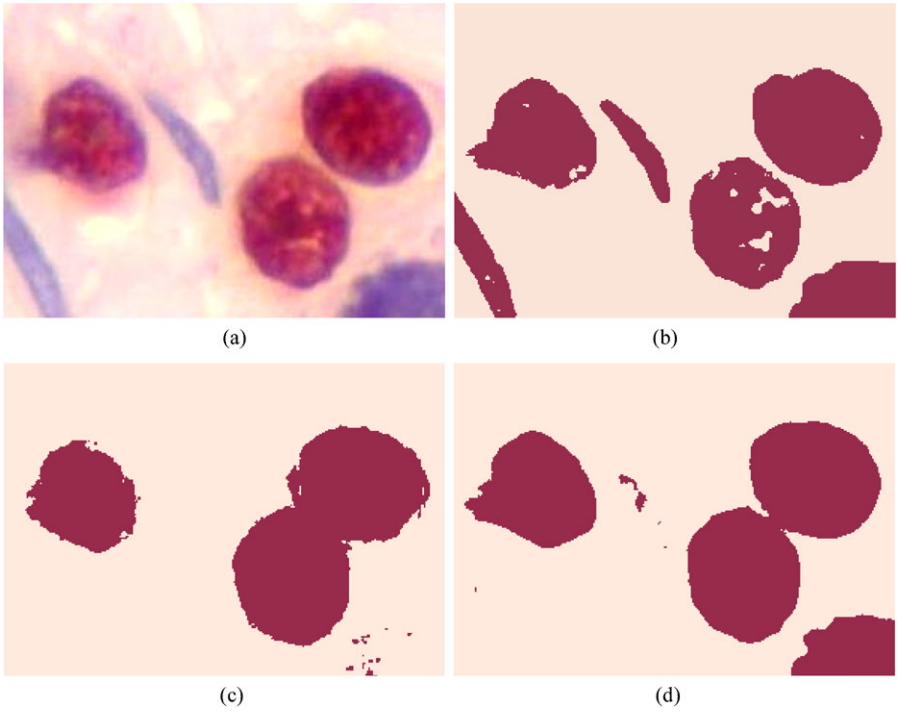

Fig. 5 (Color online) Segmentation results on a colour image, (**a**) original image with RGB representation ($256 \times 256 \times 3$) and $c = 2$, (**b**) segmentation results using PCM algorithm on *red* component, (**c**) segmentation results using PCM algorithm on *green* component, (**d**) segmentation results using PCM algorithm on *blue* component. *(The various medical images used in this paper are provided with permission from Cancer Service, Salah Azaiez Hospital, Bab Saadoun, Tunis, Tunisia)*

tively, to Figs. 6(b), (c) and (d). The cells are exactly and homogeneously segmented in Fig. 6(d), which is not the case in Fig. 6(b) and (c).

It can be seen from Table 1 that 46.31%, 23.66% and 2.54% of pixels were incorrectly segmented in Fig. 6(b), (c) and (d), respectively. In fact, the experimental result presented in Fig. 6(d) is quite consistent with the visualized colour distribution in the objects, which makes it possible to take an accurate measurement of the cells volumes [12].

In fact, the experimental results indicate that the proposed method, which uses both the information reliability and the spatial neighbourhood information for the calculation of the mass functions in the DS evidence theory, is more accurate than the traditional methods in terms of segmentation quality as denoted by the segmentation sensitivity, see Table 1.

To evaluate the performance of the proposed segmentation algorithm, its accuracy was recorded. Regarding the accuracy, Tables 1 and 2 list the segmentation sensitivity of the different methods for the data set used in the experiment.

The segmentation sensitivity [17, 18] (Sens %) is computed using

$$\text{Sens} = \frac{Np_{cc}}{N \times M} \times 100 \tag{16}$$

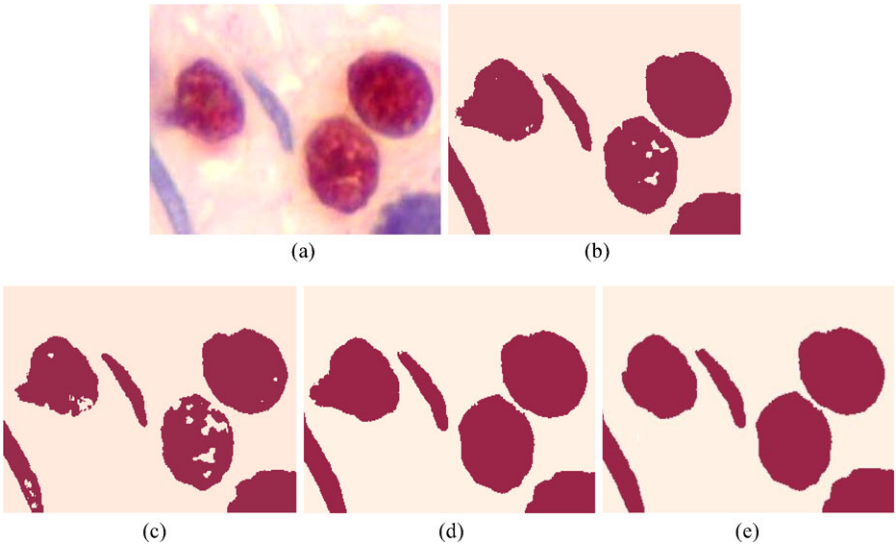

Fig. 6 (Color online) Comparison with the segmentation results on a colour image, (**a**) original image with RGB representation ($256 \times 256 \times 3$) and $c = 2$, (**b**) segmentation results where MMFD as that used for DS mass function, (**c**) segmentation results where MMFAGD as that used for DS mass function, (**d**) segmentation results based on proposed approach, and (**e**) reference segmented image

where Sens, Np_{cc} and $N \times M$ correspond to the segmentation sensitivity (%), number of correctly classified pixels and the image sizes, respectively.

The acquisition of the correct classified pixels is not a manual process; hence, software based on a reference image is run. It consists of a small program which compares the labels of the obtained pixels and the reference pixels. The correctly classified pixel denotes a pixel with a label equal to its corresponding pixel in the reference image. The labelling of the original image is generated by the user based on the image used for segmentation. Consequently, the image segmentation ground truth is generated manually by the doctor (specialist) using the original image. Figure 6(e) shows the ideal segmented image.

Since there are many incorrectly segmented pixels by the HCM and FCM based methods, some homogeneous areas are incorrectly segmented. The boundary of the green class is clearly separated by the proposed approach, while there are too many fragments in Figs. 7(b) and (c).

Since HCM and FCM based methods do not consider the spatial dependencies among the pixels and the compatibilities of the points belonging to the classes to compute the mass functions, there are some isolated pixels that are remaining. As seen in the experimental results, the proposed approach works better than the HCM and FCM based methods.

However, this new method requires a lot of computation time (see Table 3), due to the large number of iterations and the number of operations (multiplications, addition and exponent) that are necessary for the computation of membership's degree, and also for the computation of the mass functions for the simple and composite classes. On the other hand, this new method is very efficient for colour images segmentation.

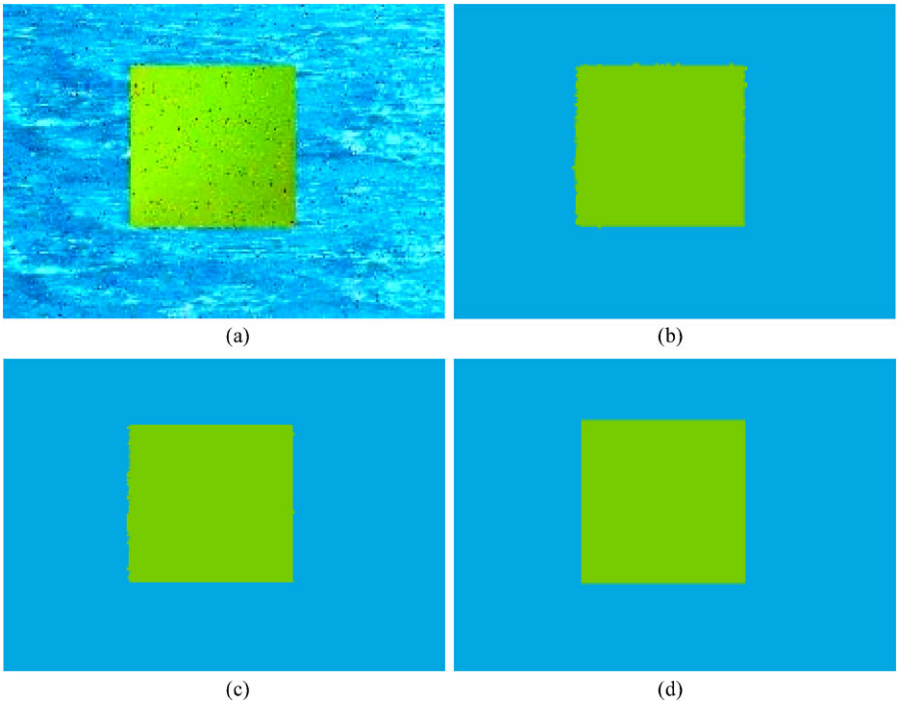

Fig. 7 (Color online) (**a**) Original image $256 \times 256 \times 3$ colour textured image disturbed with a "salt and pepper" noise and with grey level zero to 255 of each primitive colours and $c = 2$, (**b**) resulting image by HCM method, (**c**) resulting image by FCM method, (**d**) resulting image by the proposed method

To provide insights into the proposed method, we have compared the performance of the proposed method with those of the corresponding Hard and Fuzzy C-Means algorithms. The method was also tested on synthetic images and compared with other existing methods.

The comparison of the proposed approach will be presented through the next experiment. Figures 7(b), (c) and (d) shows the final segmentation results obtained from the HCM algorithm, the FCM and the PCM algorithms, respectively, when a "salt and pepper" noise of D density is added to the original image I, shown in Fig. 7(a). This affects approximately $(D \times (N \times M))$ pixels. The value of D is 0.02.

Comparing Figs. 7(c), (d), and (e), we observe that the two regions are correctly segmented in Fig 7(e), showing the complementary information provided by three primitive colours and the good estimation of the mass function by PCM.

It can be seen from Table 2 that 28.77% and 11.08% of the pixels were incorrectly segmented by HCM and FCM based methods, respectively, but only 03.13% are incorrectly segmented pixels by our proposed method. Comparing Figs. 7(b) and (c) with (d), we can see that the image resulting from the proposed method is much clearer than the one resulting from the HCM and FCM based methods.

Table 1 Segmentation sensitivity from MMFD and DS, MMFAGD and DS, and PCM and DS for the data set shown in Fig. 2

	MMFD and DS	MMFAGD and DS	PCM and DS (proposed method)
Sensitivity segmentation (%)			
Image 1	66.84	72.94	96.87
Image 2	68.23	79.66	91.75
Image 3	72.56	83.19	89.85
Image 4	85.11	88.91	97.88
Image 5	75.42	76.86	94.35
Image 6	53.69	76.34	97.46
Image 7	83.54	93.88	98.84
Image 8	66.78	79.33	99.68
Image 9	75.84	77.85	98.89
Image 10	68.23	79.66	96.87
Image 11	62.74	74.43	90.18
Image 12	45.37	68.45	98.93

Table 2 Segmentation sensitivity from HCM and DS, FCM and DS, and PCM and DS for the data set shown in Fig. 2

	HCM and DS	FCM and DS	PCM and DS (proposed method)
Sensitivity segmentation (%)			
Image 1	86.74	89.45	96.87
Image 2	61.82	88.92	91.75
Image 3	73.76	87.25	89.85
Image 4	89.21	96.68	97.88
Image 5	78.62	90.15	94.35
Image 6	62.42	79.86	97.46
Image 7	73.64	96.88	98.84
Image 8	61.48	88.79	99.68
Image 9	73.38	99.63	98.89
Image 10	71.23	88.92	96.87
Image 11	44.93	69.07	90.18
Image 12	56.87	67.31	98.93

4 Conclusion

In this paper, we have proposed a new method for the estimation of the mass functions in the Dempster–Shafer's evidence theory applied to colour image segmentation. This method consists of two steps. In the first step, the automatic estimation of mass functions in the DS evidence theory is determined from the possibility theory, which takes

Table 3 Computational complexity of the proposed method

Steps of each image to be combined	Number of operations			
	Dimension	Multiplications	Additions	Exponents
N	N.M	0	0	0
$\eta_k = \frac{\sum_{k=1}^{n} u_{ik}^{m} d_{ik}^{2}}{\sum_{k=1}^{n} u_{ik}^{2}}$	(n.1)	(n.4)	(n.2)	1
$u_{ik} = \frac{1}{1+(\frac{d_{ik}^{2}}{\eta_k})^{\frac{1}{m-1}}}$	c.n	c.n.3	c.n	1
$\|U^{(t'-1)} - U^{(t')}\| < \varepsilon$	1	0	1	0
$\overline{u_{xy}} = \frac{1}{t^2} \sum_{p=x-(t-1)/2}^{x+(t-1)/2} \sum_{q=y-(t-1)/2}^{y+(t-1)/2} u_{pq}$	$(N-2)(M-2)$	$(N-2)(M-2)$	$(N-2)(M-2)$	0
$m_{xy}(H_i) = m_{xy}(C_i) = \overline{u_{xy}}(C_i); 1 \le i \le c$	$(N-2)(M-2)$	0	0	0
$S(\overline{u_{xy}}(C_l))$	$2.(N-2)(M-2)$	0	0	0
$S(\overline{u_{xy}}(C_m))$	$2.(N-2)(M-2)$	0	0	0
$m_{xy}(H_l \cup H_m) = m_{xy}(C_l \cup C_m)$ $= \hbar(\overline{u_{xy}}(C_l)), \overline{u_{xy}}(C_m)$ $= \frac{S(\overline{u_{xy}}(C_l)).S(\overline{u_{xy}}(C_m))}{4.S_{\max}}$	$3.(N-2)(M-2)$	0	0	0
For $i = 2$; $m_{xy}(H_i) = m_{xy}^{1}(H_i) \oplus m_{xy}^{2}(H_i) \oplus m_{xy}^{3}(H_i)$	$2^2.(N-2)(M-2)$	$20.(N-2).(M-2)$	0	0

into account the compatibility information and represents the membership degree of each pixel with the central pixel and its neighbours. In the second step, the final mass functions are computed based on the evidence theory. The Dempster–Shafer's orthogonal rule is used to handle the missing information and the high correlation of the three-colour image components. The proposed method has been compared with the conventional and the automatic mass functions determination procedures. The best experimental results have been achieved by the proposed method for the following reasons. First, the proposed method uses the compatibility information to generate membership levels, i.e., the resulting partition of the data can be interpreted as the compatibilities of the points with the class prototypes, but the HCM and FCM approaches use only the grey level to determine the membership degree of each pixel. Secondly, the proposed method considers the neighbouring membership degree among the pixels of the images during the determination of a final mass function in the DS evidence theory.

Acknowledgements The authors would like to thank the Editor-in-Chief, Prof. M.N.S. Swamy, and the anonymous reviewers for their constructive comments and corrections. They also address their thanks to Professor Khaled Ben Romdhane, the head of the cancer service of Hospital Salah Azaiez Bab Saadoun, Tunis, Tunisia for providing the diverse images and for his helpful collaboration.

References

1. M.N. Ahmed, S.M. Yamany, N. Mohamed, A.A. Farag, T. Moriary, A modified fuzzy c-means algorithm for bias field estimation and segmentation of MRI data. IEEE Trans. Med. Imaging **21**, 193–199 (2002)
2. S. Anjan, B. Anjan, B. Nilanjan, B. Siddhartha, B. Kartikeyan, C. Manab, K.L. Majumder, Landcover classification in MRF context using Dempster Shafer fusion for multisensory imagery. IEEE Trans. Image Process. **14**(5), May 2005
3. I. Bloch, H. Maitre, Fusion of image information under imprecision, in *Aggregation and Fusion of Imperfect Information*, ed. by B. Bouchon-Meunier. Series Studies in Fuzziness (Springer, Berlin, 1997), pp. 189–213
4. E. Binaghi, P. Madella, Fuzzy Dempster–Shafer reasoning for rule-based classifiers. Int. J. Intell. Syst. **14**(6), 559–583 (1999)
5. J.C. Bezdek, *Pattern Recognition with Fuzzy Objective Function Algorithms* (Plenum, New York, 1981)
6. S.B. Chaabane, M. Sayadi, F. Fnaiech, E. Brassart, Estimation of the mass function in the Dempster–Shafer's evidence theory using automatic thresholding for color image segmentation, in *International Conference on Signals, Circuits and Systems*, SCS'08, Hammamet, Tunisia, 7–9 November 2008
7. S.B. Chaabane, M. Sayadi, F. Fnaiech, E. Brassart, Color image segmentation based on Dempster–Shafer evidence theory, in *IEEE Mediterranean Electrotechnical Conference, MELECON'2008*, Ajaccio, France, 5–7 Mai 2008
8. S.B. Chaabane, M. Sayadi, F. Fnaiech, E. Brassart, Colour image segmentation using homogeneity approach and data fusion techniques. EURASIP J. Adv. Signal Process. **2010**, 367297 (2010)
9. S.B. Chaabane, M. Sayadi, F. Fnaiech, E. Brassart, Dempster–Shafer evidence theory for image segmentation: application in cells images. Int. J. Signal Process. **5**, 126–132 (2009)
10. H.D. Cheng, X.H. Jiang, Y. Sun, J. Wang, Colour image segmentation: advances and prospects. Pattern Recognit. **34**, 2259–2281 (2001)
11. R.E. Cummings, P. Pouliquen, M.A. Lewis, A vision chip for color segmentation and pattern matching. EURASIP J. Appl. Signal Process. **7**, 703–712 (2003)
12. O. Colot et al., *A Colour Image Processing Method for Melanoma Detection*. Lecture Notes in Computer Science (Springer, Berlin, 1998)
13. D. Dubois, Belief structures: Possibility theory and decomposable confidence measures on finite sets. Comput. Artif. Intell. **5**(5), 403–416 (1986)

14. A. Dempster, Upper and lower probabilities induced by multivalued mapping. Ann. Math. Stat. **38**, 325–339 (1967)
15. T. Denoeux, A k-nearest neighbour classification rule based on Dempster–Shafer theory. IEEE Trans. Syst. Man Cyb. **25**(5), 804–813 (1995)
16. R. Duda, P. Hart, *Pattern Classification and Scene Analysis* (Wiley, New York, 1973)
17. R.O. Duda, P.E. Hart, D.G. Sork, *Pattern Classification* (Wiley, New York, 2000)
18. V. Grau, A.U.J. Mewes, M. Alcaniz, R. Kikinis, S.K. Warfield, Improved watershed transform for medical image segmentation using prior information. IEEE Trans. Med. Imaging **23**(4), 447–458 (2004)
19. M.J. Kwon, Y.J. Han, I.H. Shin, H.W. Park, Hierarchical fuzzy segmentation of brain MR images. Int. J. Imaging Syst. Technol. **13**, 115–125 (2003)
20. C. Lucas, B.N. Araabi, Generalization of the Dempster–Shafer theory: A fuzzy-valued measure. IEEE Trans. Fuzzy Syst. **7**(3), 255–270 (1999)
21. X. Li, L. Li, H. Lu, D. Chen, Z. Liang, In homogeneity c-mean algorithm. Proc. SPIE **5032**, 995–1005 (2003)
22. A.W.C. Liew, S.H. Leung, W.H. Lau, Fuzzy image clustering incorporating spatial continuity. IEE Proc. Vis. Image Signal Process. **147**, 185–192 (2000)
23. E. Navon, O. Miller, A. Averbuch, Color image segmentation based on adaptive local thresholds. Image Vis. Comput. **23**(1), 69–85 (2005)
24. D.R. Peddle, An empirical comparison of evidential reasoning linear discriminant analysis and maximum likelihood algorithms for alpine land cover classification. Can. J. Remote Sens. **19**, 31–44 (1993)
25. K. Raghu, J.M. Keller, A possibilistic approach to clustering. IEEE Trans. Fuzzy Syst. **1**(2), 98–110 (1993)
26. F.Y. Shih, S. Cheng, Automatic seeded region growing for color image segmentation. Image Vis. Comput. **23**(10), 877–886 (2005)
27. P. Smets, The disjunctive rule of combination and the generalized Bayesian theorem. Int. J. Approx. Reason. **9**, 1–35 (1993)
28. G. Shafer, *A Mathematical Theory of Evidence* (Princeton University Press, Princeton, 1976)
29. P. Vannoorenberghe, O. Colot, D.D. Brucq, Color image segmentation using Dempster–Shafer's theory, in *Proc. ICIP'99*, pp. 300–304, October, 1999
30. R.R. Yager, A class of fuzzy measures generated from a Dempster–Shafer belief structure. Int. J. Intell. Syst **14**, 1239–1247 (1999)
31. H.J. Zimmerman, P. Zysno, Quantifying vagueness in decision models. Eur. J. Oper. Res. **22**, 148–158 (1985)
32. Y.M. Zhu, O. Dupuis, M. Rombaut, Automatic determination of mass functions in Dempster–Shafer theory using fuzzy c-means and spatial neighborhood information for image segmentation. Opt. Eng. **41**(4), 760–771 (2002)